

Sterile neutrino dark matter in conformal Majoron models

João Gonçalves,^a Danny Marfatia,^b António P. Morais^{c,a} Vinícius Oliveira^{a,c,f} and Roman Pasechnik^f

^aLaboratório de Instrumentação e Física Experimental de Partículas (LIP), Universidade do Minho, 4710-057 Braga, Portugal

^bDepartment of Physics and Astronomy, University of Hawaii at Manoa, Honolulu, HI 96822, USA

^cDepartamento de Física, Escola de Ciências, Universidade do Minho, 4710-057 Braga, Portugal

^dDepartamento de Física da Universidade de Aveiro, Campus de Santiago, 3810-183 Aveiro, Portugal.

^fDepartment of Physics, Lund University, 221 00 Lund, Sweden

E-mail: jpedropino@ua.pt, dmarf8@hawaii.edu, amorais@fisica.uminho.pt, viniciuslbo@lip.pt, roman.pasechnik@fysik.lu.se

Abstract. We study sterile neutrino dark matter (DM) in a classically conformal $U(1)'$ extension of the Standard Model with three right-handed neutrinos and a Majoron-like singlet scalar that generate the observed pattern of active neutrino masses and mixing via the type-I seesaw mechanism. Working in the regime of strongly suppressed active-sterile mixing, we show that the observed DM abundance can be produced through freeze-in from feeble interactions mediated by the heavy Z' and the conformal scalar. We solve the Boltzmann equation for the nonthermal phase-space distribution and confront the scenario with Lyman- α data by computing the matter power spectrum. For keV-scale sterile neutrinos we identify the viable parameter space consistent with structure-formation and X-ray bounds, including regions compatible with a tentative 3.5 keV line. If a second sterile state is long-lived, late decays can realize a two-component setup that alleviates the S_8 tension. In a highly fine-tuned variant of the model, the 220 PeV KM3NeT event can also be explained by invoking the decay of a superheavy sterile neutrino.

Contents

1	Introduction	1
2	Theoretical setup	2
2.1	Neutrino sector	2
2.2	Scalar sector	4
2.3	Gauge sector	4
3	Stability and decay of keV sterile neutrinos	5
4	Freeze-in production and relic abundance of keV dark matter	6
5	Lyman-α constraints	9
6	3.5 keV X-ray line	10
7	Multi-component decaying dark matter and the S_8 tension	12
8	The KM3NeT event	14
9	Summary	15
A	Production cross sections for light dark matter	16

1 Introduction

Sterile neutrinos are well-motivated dark matter (DM) candidates that span a wide range of masses and have a variety of production histories; see Ref. [1] for a review. In the keV mass window, a sterile neutrino N is intrinsically unstable due to its mixing with active neutrinos, and can produce observable X-ray signals through the radiative decay $N \rightarrow \nu\gamma$ [2]. This motivates dedicated line searches with current and forthcoming X-ray missions such as *Athena* [3], *eROSITA* [4] and *XRISM* [5]. In fact, a weak feature at $E_\gamma \simeq 3.5$ keV reported in stacked cluster data and in observations of individual objects – including the Perseus cluster and M31 – triggered sustained interest in a sterile neutrino interpretation with $m_N \simeq 7$ keV and small active-sterile neutrino mixing $\sin^2 2\theta_{\text{eff}} \sim 10^{-10}$ [6, 7]. A signal near the same energy has also been observed in the galactic center of the Milky Way in deep *XMM-Newton* exposures [8].

It is well known that light DM candidates produced via thermal freeze-out in the early Universe typically suffer from an overabundance problem. Perhaps the simplest nonthermal production mechanism for sterile neutrino DM is nonresonant production via active-sterile oscillations in the thermal plasma, the so-called Dodelson-Widrow (DW) mechanism [9, 10]. However, with this mechanism, the inferred DM relic abundance cannot be saturated by sterile neutrinos with masses below 41 keV (at 95% C.L.), a conclusion drawn from a combination of X-ray [11–18] and Lyman- α forest data [19–21]. The latter are sensitive to the phase-space distribution of sterile neutrinos and constrain their relic abundance for masses between 1 keV to 8 keV [21–23].

The status of the 3.5 keV line mentioned above has been extensively scrutinized, including with follow-up searches and alternative (astrophysical/instrumental) explanations [1, 14, 17, 18, 24–28]. Recent high-resolution spectroscopy continues to sharpen constraints on putative unidentified lines. For example, a stacked *XRISM*/Resolve analysis of ten galaxy clusters reports no statistically significant novel features in the 2.5 keV – 15 keV window and sets upper limits on the decay interpretation of the 3.5 keV line [27]. Furthermore, Ref. [28] finds no significant evidence for the line in attempts to reproduce previous analyses of various datasets, and instead finds evidence for background mismodeling in several analyses. Rather than address the controversy, in a part of our study we take the optimistic view that claims for the 3.5 keV

line are legitimate. Since the DW mechanism is now strongly constrained, we explore a DM freeze-in production scenario. We focus on an extremely suppressed active-sterile mixing, $\sin^2 2\theta_{\text{eff}} \ll 10^{-10}$ in which DW production is negligible.

We study sterile neutrino DM in a class of *classically conformal* gauged $U(1)'$ extensions of the Standard Model (SM). Three sterile neutrinos are required for anomaly cancellation, and neutrino masses are generated via a type-I seesaw mechanism [29]. The conformal setup triggers spontaneous symmetry breaking radiatively via the Coleman-Weinberg mechanism, and the $U(1)'$ breaking scale generates Majorana masses for three SM-singlet neutrinos. The lightest sterile state, denoted N_1 , can play the role of a nonthermal DM candidate. In the keV domain, we compute the freeze-in abundance and apply small-scale structure constraints by propagating the resulting nonthermal phase-space distribution through a Boltzmann solver for cosmological perturbations. We also determine the parameter regions where radiative decays of N_1 can yield an observable X-ray line.

A persistent mild discrepancy exists between the amplitude of late-time matter fluctuations inferred from early-Universe observations (most notably Planck) and that preferred by low-redshift large-scale structure probes [30–32]; the latter measure a smaller value than does Planck. This is widely known as the S_8 tension, where $S_8 \equiv \sigma_8 \sqrt{\Omega_m/0.3}$, with σ_8 denoting the variance of matter fluctuations on 8 Mpc/h scales and Ω_m the present matter density parameter; see e.g. [33] for a review. We address this tension in our framework with two keV mass sterile neutrinos, with one decaying to the other. The lighter neutrino receives a small momentum kick sufficient for it to freestream and suppress power on small scales.

Finally, we briefly comment on how these models accommodate a very heavy sterile neutrino that may explain the recently reported ~ 200 PeV KM3NeT event [34] via its decay [35].

The article is organized as follows. In Section 2 we introduce the classically conformal $U(1)'$ Majoron-type model and specify its neutrino, scalar, and gauge sectors. In Section 3 we discuss the cosmological stability requirements for keV sterile neutrinos and summarize the relevant decay channels and lifetimes. In Section 4 we present the freeze-in production mechanism and the computation of the relic abundance. In Section 5 we confront the resulting nonthermal DM spectrum with Lyman- α forest constraints. The phenomenology of the 3.5 keV X-ray line and its interpretation in terms of $N_1 \rightarrow \nu\gamma$ is addressed in Section 6. In Section 7 we demonstrate how a multi-component (decaying) DM realization resolves the S_8 tension. In Section 8 we comment on how the decay of a super-heavy sterile neutrino can explain the KM3NeT event. We summarize our findings in Section 9.

2 Theoretical setup

We work within a class of classically conformal, anomaly-free gauged $U(1)'$ extensions of SM supplemented by three right-handed neutrinos N_I ($I = 1, 2, 3$) required by anomaly cancellation, and a complex SM-singlet scalar σ that generate neutrino masses [36–38]. Classical conformal invariance forbids explicit mass terms in the tree-level Lagrangian; all mass scales arise from radiative symmetry breaking via the Coleman-Weinberg mechanism and the induced vacuum expectation values (VEVs). The model setup and the one-loop treatment of the scalar sector follow Ref. [39].

Throughout, we parametrize the flavor-universal $U(1)'$ charges in terms of the charges $x_{\mathcal{H}}$ and x_{σ} of the SM Higgs doublet \mathcal{H} and σ , respectively. The remaining charge assignments are fixed by gauge invariance of the Yukawa sector and by anomaly cancellation. The resulting field content and charges are provided in Table 1.

2.1 Neutrino sector

The neutrino Yukawa Lagrangian reads [36–38]

$$\mathcal{L}_{\nu} \supset y_{\nu}^{ij} \overline{L_i} \tilde{\mathcal{H}} N_j + y_{\sigma}^I \overline{N_I^c} N_I \sigma + \text{h.c.}, \quad (2.1)$$

where $L_i = (\nu_{Li}, e_{Li})^T$, $i, j = 1, 2, 3$, is the SM lepton doublet, and $\tilde{\mathcal{H}} = i\sigma_2 \mathcal{H}^*$. After symmetry breaking,

$$\langle \mathcal{H} \rangle = \frac{1}{\sqrt{2}} \begin{pmatrix} 0 \\ v \end{pmatrix}, \quad \langle \sigma \rangle = \frac{v_{\sigma}}{\sqrt{2}}, \quad (2.2)$$

Field	$\mathbf{U}(1)'$	$\mathbf{SU(3)}_c$	$\mathbf{SU(2)}_L$	$\mathbf{U(1)}_Y$
Q	$\frac{1}{3}x_{\mathcal{H}} + \frac{1}{6}x_{\sigma}$	3	2	1/6
u_R	$\frac{4}{3}x_{\mathcal{H}} + \frac{1}{6}x_{\sigma}$	3	1	2/3
d_R	$-\frac{2}{3}x_{\mathcal{H}} + \frac{1}{6}x_{\sigma}$	3	1	-1/3
L	$-x_{\mathcal{H}} - \frac{1}{2}x_{\sigma}$	1	2	-1/2
e_R	$-2x_{\mathcal{H}} - \frac{1}{2}x_{\sigma}$	1	1	-1
\mathcal{H}	$x_{\mathcal{H}}$	1	2	1/2
N	$-\frac{1}{2}x_{\sigma}$	1	1	0
σ	x_{σ}	1	1	0

Table 1: Field content and gauge charges in the conformal $\mathbf{U}(1)'$ framework. All $\mathbf{U}(1)'$ charges are expressed in terms of the Higgs charge $x_{\mathcal{H}}$ and singlet charge x_{σ} ; the other assignments follow from gauge invariance and anomaly cancellation.

where $v \simeq 246$ GeV and v_{σ} is generated radiatively. In the basis (ν_L, N^c) the 6×6 Majorana mass matrix is

$$\mathbf{M}_{\nu} = \begin{pmatrix} 0 & \frac{v}{\sqrt{2}} \mathbf{y}_{\nu}^T \\ \frac{v}{\sqrt{2}} \mathbf{y}_{\nu} & \frac{v_{\sigma}}{\sqrt{2}} \mathbf{y}_{\sigma} \end{pmatrix}. \quad (2.3)$$

Assuming a standard type-I seesaw hierarchy $\|\frac{v}{\sqrt{2}} \mathbf{y}_{\nu}\| \ll \|\frac{v_{\sigma}}{\sqrt{2}} \mathbf{y}_{\sigma}\|$, the light neutrino mass matrix is

$$\mathbf{m}_{\nu} \simeq \frac{1}{\sqrt{2}} \frac{v^2}{v_{\sigma}} \mathbf{y}_{\nu}^T \mathbf{y}_{\sigma}^{-1} \mathbf{y}_{\nu}, \quad (2.4)$$

whose eigenvalues correspond to the three active neutrinos m_1, m_2, m_3 . The heavy neutrino mass matrix is

$$\mathbf{M}_N \simeq \frac{v_{\sigma}}{\sqrt{2}} \mathbf{y}_{\sigma}, \quad (2.5)$$

with eigenstates denoted by N_I with masses M_{N_I} . We identify the lightest sterile state N_1 as the DM candidate. In the keV-scale scenarios studied below we take $M_{N_1} \in [1, 100]$ keV, while M_{N_2} and M_{N_3} are treated as free parameters (with special attention to the case where N_2 is also long-lived).

For parameter scans it is convenient to parameterize the Dirac Yukawa matrix using the Casas-Ibarra construction [40]. The type-I seesaw relation (2.4) can be written as

$$\mathbf{m}_{\nu} \simeq \mathbf{y}_{\nu}^T \boldsymbol{\Sigma} \mathbf{y}_{\nu}, \quad \boldsymbol{\Sigma} \equiv \frac{1}{\sqrt{2}} \frac{v^2}{v_{\sigma}} \mathbf{y}_{\sigma}^{-1} = \frac{v^2}{2} \mathbf{M}_N^{-1}, \quad (2.6)$$

with [41]

$$\mathbf{y}_{\nu} = i \boldsymbol{\Sigma}^{-1/2} \mathbf{R} \mathbf{D}_{\sqrt{m}} \mathbf{U}_{\text{PMNS}}^{\dagger}, \quad (2.7)$$

where $\mathbf{D}_{\sqrt{m}} = \text{diag}(\sqrt{m_1}, \sqrt{m_2}, \sqrt{m_3})$, \mathbf{U}_{PMNS} is the Pontecorvo-Maki-Nakagawa-Sakata (PMNS) mixing matrix, and \mathbf{R} is a complex orthogonal matrix that satisfies $\mathbf{R}^T \mathbf{R} = \mathbf{1}$. In the heavy neutrino mass basis, $\boldsymbol{\Sigma}$ is diagonal with eigenvalues, $\Sigma_I = v^2/(2M_{N_I})$. The matrix \mathbf{R} can be parameterized as a product of three 3D complex rotations \mathbf{R}_{iI} in each iI -plane, i.e., $\mathbf{R} = \mathbf{R}_{23}(z_1) \mathbf{R}_{13}(z_2) \mathbf{R}_{12}(z_3)$, with complex angles z_k . This parameterization guarantees compatibility with the measured active neutrino masses and mixing angles while allowing a broad exploration of the sterile sector. As a phenomenological input, we utilize the results of NuFIT [42] for the neutrino mass differences and PMNS mixing angles and apply the cosmological bound on the sum of active neutrino masses, $\sum_{i=1,2,3} m_i < 0.12$ eV [43].

2.2 Scalar sector

The classically conformal tree-level scalar potential reads

$$V_0(\mathcal{H}, \sigma) = \lambda_h(\mathcal{H}^\dagger \mathcal{H})^2 + \lambda_\sigma(\sigma^* \sigma)^2 + \lambda_{\sigma h}(\mathcal{H}^\dagger \mathcal{H})(\sigma^* \sigma). \quad (2.8)$$

\mathcal{H} and σ develop nonzero VEVs upon radiative symmetry breaking. In a conformal setting, one scalar degree of freedom is massless at tree level along the flat direction and can be identified as the Goldstone boson of spontaneously broken scale invariance. Radiative corrections explicitly break the scale invariance via the Coleman–Weinberg (CW) mechanism by lifting the flat direction of the tree-level potential, thus generating a nonzero pseudo-Goldstone mass term.

Expanding the fields about the vacuum as

$$\mathcal{H} = \frac{1}{\sqrt{2}} \begin{pmatrix} 0 \\ v + h \end{pmatrix}, \quad \sigma = \frac{1}{\sqrt{2}} (v_\sigma + s) e^{iJ/v_\sigma}, \quad (2.9)$$

the spectrum contains a physical CP-even state dominantly aligned with the SM Higgs h_1 , a singlet-like CP-even state h_2 , and a CP-odd Majoron J providing the longitudinal mode of the Z' boson. The CP-even fields (h, s) are related to mass eigenstates (h_1, h_2) by an orthogonal rotation,

$$\begin{pmatrix} h_1 \\ h_2 \end{pmatrix} = \mathcal{O} \begin{pmatrix} h \\ s \end{pmatrix}, \quad \mathcal{O} = \begin{pmatrix} \cos \alpha & \sin \alpha \\ -\sin \alpha & \cos \alpha \end{pmatrix}. \quad (2.10)$$

In our framework, we identify h_1 with the observed SM-like Higgs boson, with tree-level mass, $M_{h_1} \approx \sqrt{-\lambda_{\sigma h}} v_\sigma \simeq 125.11$ GeV [44], and the heavier scalar h_2 is aligned with the pseudo-Goldstone boson of scale symmetry breaking with mass generated radiatively at one loop level.

We follow Ref. [39] for the one-loop effective potential, tadpole conditions, and mass renormalization. First, we evaluate the tadpole equations and the scalar mass spectrum at the one-loop level by including the CW potential V_{CW} , in the total potential $V_{\text{tot}} = V_0 + V_{\text{CW}}$, and then determine the scalar mass spectrum by incorporating finite-momentum corrections due to self-energies. This procedure allows us to determine λ_σ and $\lambda_{\sigma h}$ through the one-loop tadpole conditions, and λ_h and v_σ from the one-loop corrected scalar masses, leaving the mass of the heavy scalar M_{h_2} as the only free parameter in the scalar sector. Higgs signal-strength measurements and direct searches for additional scalars constrain $|\sin \alpha| < 0.3$ [45]. The phenomenologically viable parameter space relevant for freeze-in DM corresponds to large $U(1)'$ breaking scales, $v_\sigma > 1$ TeV, with a strongly suppressed scalar mixing angle, $|\sin \alpha| \ll 10^{-3}$. The coupling of h_1 to light N_1 induced by mixing $\propto M_{N_1} \sin \alpha / v_\sigma$ and yields invisible Higgs decay with width

$$\Gamma_{h_1 \rightarrow \bar{N}_1 N_1} = \frac{M_{N_1}^2}{8\pi v_\sigma^2} \sin^2 \alpha M_{h_1} \left(1 - \frac{4M_{N_1}^2}{M_{h_1}^2} \right)^{3/2}. \quad (2.11)$$

We will find this to be negligible compared to the SM Higgs boson width.

2.3 Gauge sector

The $U(1)'$ gauge field B'_μ couples to the $U(1)'$ current with coupling g_L , and gauge invariance allows kinetic mixing between the $U(1)'$ field strength $B'_{\mu\nu}$ and the hypercharge field strength $B_{\mu\nu}$. We parameterize the mixing at the level of covariant derivatives by introducing an effective mixing parameter g_{12} [39]. After electroweak and $U(1)'$ breaking, the neutral gauge boson mass-squared matrix in the (B_μ, A_μ^3, B'_μ) basis reads

$$\mathcal{M}_V^2 = \begin{pmatrix} \frac{1}{4}g_2^2 v^2 \tan^2 \theta_W & -\frac{1}{4}g_2^2 v^2 \tan \theta_W & \frac{1}{4}g_2 v^2 \tan \theta_W (g_{12} + 2g_L x_{\mathcal{H}}) \\ -\frac{1}{4}g_2^2 v^2 \tan \theta_W & \frac{1}{4}g_2^2 v^2 & -\frac{1}{4}g_2 v^2 (g_{12} + 2g_L x_{\mathcal{H}}) \\ \frac{1}{4}g_2 v^2 \tan \theta_W (g_{12} + 2g_L x_{\mathcal{H}}) & -\frac{1}{4}g_2 v^2 (g_{12} + 2g_L x_{\mathcal{H}}) & g_L^2 v_\sigma^2 x_\sigma^2 + \frac{1}{4}v^2 (g_{12} + 2g_L x_{\mathcal{H}})^2 \end{pmatrix}, \quad (2.12)$$

where θ_W is the Weinberg angle and g_2 is the $SU(2)_L$ gauge coupling. Thus, g_L , g_{12} , $x_{\mathcal{H}}$ and x_σ are free parameters that fully determine the gauge sector. Diagonalization yields a massless photon and two

massive states identified with the Z^0 boson of the SM and a massive Z' vector boson; expressions for their masses can be found in Ref. [39].

It is well known that light DM particles produced via freeze-out suffer from an overabundance problem. To avoid this issue, we focus on the regime in which the DM never reaches thermal equilibrium, and is produced nonthermally via the freeze-in mechanism. We are interested in the limit $g_L, g_{12} \ll 1$ and $v_\sigma \gg v$, in which case

$$M_Z^2 \simeq \frac{1}{4} g_2^2 (1 + \tan^2 \theta_W) v^2, \quad M_{Z'}^2 \simeq (g_L x_\sigma v_\sigma)^2. \quad (2.13)$$

We require $M_{Z'} \gtrsim 5$ TeV to satisfy bounds from the LHC [46–48]. In conformal $U(1)'$ models, $\lambda_\sigma \sim g_L^4$ [49], so that small g_L simultaneously helps satisfy collider bounds and ensures the hierarchy $M_{h_2} < M_{Z'}$ which is needed in the DM production analysis below.

3 Stability and decay of keV sterile neutrinos

The DM candidate N_1 is not absolutely stable. It inherits weak interactions through its mixing with the active neutrinos. Let U denote the unitary matrix that diagonalizes the neutrino mass matrix in Eq. (2.3), such that the active flavor states contain a small admixture of sterile states. For the lightest sterile neutrino N_1 , we define an effective active-sterile mixing parameter,

$$\sin^2 \theta_{\text{eff}} \equiv \sum_{\alpha=e,\mu,\tau} |U_{\alpha(I=1)}|^2 \ll 1, \quad (3.1)$$

which determines the primary SM-induced decay channels. In the seesaw regime, $U_{\alpha(I=1)} \simeq (m_D)_{\alpha(I=1)} / M_{N_1}$. For keV N_1 , θ_{eff} is tiny because the Dirac neutrino mass scale $m_D = v y_\nu / \sqrt{2}$. This enables the N_1 lifetime to exceed the age of the Universe, $\tau_0 \simeq 13 \times 10^9$ yr.

Light N_1 mainly decay via the two-body $N_1 \rightarrow \nu \gamma$ and the three-body invisible $N_1 \rightarrow \nu \nu \bar{\nu}$ channels [50]. The one-loop contribution to the radiative $N_1 \rightarrow \nu \gamma$ decay width is induced by W -exchange and given by [2, 51, 52]

$$\Gamma_{N_1 \rightarrow \nu \gamma} \simeq \frac{9 \alpha_{\text{EM}} G_F^2}{256 \pi^4} \sin^2 \theta_{\text{eff}} M_{N_1}^5 \simeq 5.5 \times 10^{-22} \sin^2 \theta_{\text{eff}} \left(\frac{M_{N_1}}{1 \text{ keV}} \right)^5 \text{ s}^{-1}, \quad (3.2)$$

where α_{EM} is the fine-structure constant and G_F is the Fermi constant. This channel produces a mono-energetic photon at $E_\gamma \simeq M_{N_1}/2$ and is therefore tightly constrained by X-ray line searches. With $M_{N_1} \sim \mathcal{O}(\text{keV})$, the corresponding bounds typically require $\sin^2 \theta_{\text{eff}} \lesssim 10^{-10} \text{--} 10^{-11}$, depending on the dataset, implying lifetimes $\tau_{N_1} \equiv \Gamma_{N_1}^{-1}$ well above cosmological timescales. In our model, an additional contribution to $\Gamma_{N_1 \rightarrow \nu \gamma}$ arises due to kinetic mixing between $U(1)_Y$ and $U(1)'$. However, this contribution is subleading in the regime of small $g_{12}, g_L \ll 1$ despite being generated at tree level. Finally, the mass mixing-induced three-body decay proceeds via an off-shell Z^0 boson and yields [51]

$$\Gamma_{N_1 \rightarrow 3\nu} \simeq \frac{G_F^2}{96 \pi^3} \sin^2 \theta_{\text{eff}} M_{N_1}^5, \quad (3.3)$$

which we evaluated with `MadGraph` [53]. Requiring that the corresponding lifetime is longer than the age of the Universe gives [10]

$$\sin^2 \theta_{\text{eff}} < 1.1 \times 10^{-7} \left(\frac{50 \text{ keV}}{m_{N_1}} \right)^5. \quad (3.4)$$

This decay channel is invisible and dominant compared to the radiative loop-induced channel:

$$\frac{\Gamma_{N_1 \rightarrow \nu \gamma}^{(1 \text{ loop})}}{\Gamma_{N_1 \rightarrow 3\nu}} \simeq \frac{27 \alpha_{\text{EM}}}{8\pi} \sim \mathcal{O}(10^{-2}). \quad (3.5)$$

Thus, the total decay width of N_1 can be approximated as

$$\Gamma_{N_1} \simeq \Gamma_{N_1 \rightarrow 3\nu} + \Gamma_{N_1 \rightarrow \nu\gamma}. \quad (3.6)$$

In practice, the DM stability bound translates into a bound on the decay width, $\Gamma_{N_1} < \tau_0^{-1} = 1.5 \times 10^{-42}$ GeV, which we enforce in our numerical search for viable parameter space regions together with the current X-ray constraints. The latter impose an upper bound on the neutrino mixing, $\sin^2 2\theta_{\text{eff}} \ll 10^{-10}$ [54], which in turn restricts the z_i angles in the \mathbf{R} matrix of Eq. (2.7) to have magnitudes $|z_i| \lesssim 10^{-4}$.

4 Freeze-in production and relic abundance of keV dark matter

Since $\sin^2(2\theta_{\text{eff}}) \lesssim 10^{-10}$, the abundance of DM produced through DW can be neglected. In addition, self-interactions are highly suppressed due to the large masses of the mediators h_2 and Z' . In this regime, the interactions connecting the $U(1)'$ sector to the SM are so feeble that the lightest sterile neutrino N_1 never attains thermal equilibrium with the SM plasma, and its cosmological abundance is produced gradually through the so-called *freeze-in* mechanism [55]. In this scenario, initially no dark particles are present, and rare scatterings among bath particles continuously generate a small population of N_1 states until the temperature of the Universe falls well below the relevant reaction thresholds. In what follows, we investigate the conditions needed to reproduce the observed relic abundance assuming, for simplicity, no initial abundance of DM while ensuring stability and consistency with current cosmological and astrophysical bounds.

Assuming a standard radiation-dominated cosmology and an SM thermal bath in equilibrium, the number density of a sterile species N_I produced dominantly via $2 \rightarrow 2$ annihilation processes is governed by the Boltzmann equation,

$$\dot{n}_{N_I} + 3Hn_{N_I} = \Gamma(\text{SM SM} \rightarrow N_I N_I) - \Gamma(N_I N_I \rightarrow \text{SM SM}), \quad (4.1)$$

where $\Gamma(\text{SM SM} \rightarrow N_I N_I)$ and $\Gamma(N_I N_I \rightarrow \text{SM SM})$ are the N_I production and annihilation rates per unit volume, respectively. The Hubble rate at temperature T in the radiation era is

$$H(T) = \sqrt{\frac{\pi^2}{90} g_\rho(T)} \frac{T^2}{M_{\text{Pl}}}, \quad (4.2)$$

with $M_{\text{Pl}} = 2.44 \times 10^{18}$ GeV the reduced Planck mass, and $g_\rho(T)$ the effective number of energetic degrees of freedom.

For the Maxwell-Boltzmann distribution function, the reaction rate per unit volume can be written as

$$\Gamma(\text{SM SM} \rightarrow N_I N_I) = \langle \sigma(\text{SM SM} \rightarrow N_I N_I) v_r \rangle (n_{\text{SM}}^{\text{eq}})^2, \quad (4.3)$$

where $\langle \sigma(\text{SM SM} \rightarrow N_I N_I) v_r \rangle$ denotes the thermal average of the production cross section times the relative velocity. Hence, the interaction rate is given by

$$\mathcal{R}(\text{SM SM} \rightarrow N_I N_I) = \frac{\Gamma(\text{SM SM} \rightarrow N_I N_I)}{n_{\text{SM}}^{\text{eq}}}. \quad (4.4)$$

The Maxwell-Boltzmann equilibrium number densities for the SM particles and N_I are given by

$$n_{\text{SM}}^{\text{eq}} = \frac{g_{\text{SM}}}{2\pi^2} M_{\text{SM}}^2 T K_2(M_{\text{SM}}/T), \quad n_{N_I}^{\text{eq}} = \frac{g_N}{2\pi^2} M_{N_I}^2 T K_2(M_{N_I}/T), \quad (4.5)$$

where g_{SM} is the number of internal degrees of freedom of the SM particle, $g_N = 2$ for Majorana fermions, and $K_2(x)$ is the modified Bessel function of the second kind.

In the freeze-in regime, $\Gamma(N_I N_I \rightarrow \text{SM SM}) \ll \Gamma(\text{SM SM} \rightarrow N_I N_I)$, and Eq. (4.1) reduces to

$$\dot{n}_{N_I} + 3Hn_{N_I} \simeq \Gamma(\text{SM SM} \rightarrow N_I N_I). \quad (4.6)$$

Switching to the comoving yield $Y_{N_I} \equiv n_{N_I}/s$ and the dimensionless inverse temperature $x \equiv M_{N_I}/T$ leads to

$$\frac{dY_{N_I}}{dx} = \sqrt{\frac{8\pi^2 M_{\text{Pl}}^2}{45}} \frac{g_*^{1/2} M_{N_I}}{x^2} \langle \sigma(\text{SM SM} \rightarrow N_I N_I) v_r \rangle (Y_{\text{SM}}^{\text{eq}})^2 \simeq \frac{s}{Hx} \langle \sigma(\text{SM SM} \rightarrow N_I N_I) v_r \rangle (Y_{\text{SM}}^{\text{eq}})^2, \quad (4.7)$$

where $s(T) = (2\pi^2/45) g_s(T) T^3$ is the entropy density, $g_s(T)$ is the effective number of entropic degrees of freedom, and

$$Y_{N_I}^{\text{eq}}(x) = \frac{45}{4\pi^4} \frac{g_N}{g_s} x^2 K_2(x), \quad g_*^{1/2} \equiv \frac{g_s}{g_\rho^{1/2}} \left(1 + T \frac{dg_s/dT}{3g_s} \right). \quad (4.8)$$

The approximate equality in Eq. (4.7) is obtained by neglecting a subleading derivative term $\propto dg_s/dT$. Furthermore, the thermal averaged production cross section is [56]

$$\langle \sigma(\text{SM SM} \rightarrow N_I N_I) v_r \rangle = \frac{T}{2(2\pi)^4 (n_{\text{SM}}^{\text{eq}})^2} \int_{s_{\text{min}}}^{\infty} ds \sigma(s) (s - 4M_{\text{SM}}^2) \sqrt{s} K_1(\sqrt{s}/T). \quad (4.9)$$

Here, $\sigma(s)$ denotes the total SM SM $\rightarrow N_I N_I$ production cross section evaluated at invariant mass squared s and summed over all kinematically accessible SM final states. We take $s_{\text{min}} = \max(4M_{N_I}^2, 4M_{\text{SM}}^2)$ to enforce kinematic thresholds explicitly. The present-day relic density is obtained in terms of the asymptotic yield $Y_{N_I}^{\infty}$:

$$\Omega_{N_I} h^2 = \frac{M_{N_I} s_0}{\rho_c / h^2} Y_{N_I}^{\infty} \simeq 2.745 \times 10^8 \left(\frac{M_{N_I}}{\text{GeV}} \right) Y_{N_I}^{\infty}, \quad (4.10)$$

where $s_0 = 2891.2 \text{ cm}^{-3}$ is the entropy density today, and $\rho_c = 1.053 \times 10^{-5} h^2 \text{ GeV cm}^{-3}$ is the critical density [57].

In our model, N_I is produced through annihilation of SM states into $N_I N_I$ via heavy s -channel mediators: the Z' and the Majoron-like h_2 . The dominant contributions arise from

$$\text{SM SM} \longleftrightarrow N_I N_I, \quad \text{SM SM} = \{ f\bar{f}, h_1 h_1, VV, \dots \}, \quad (4.11)$$

where f and V denote SM fermions and gauge bosons, respectively. Their relative importance depends on $M_{Z'}$, M_{h_2} , g_L , and the scalar-sector parameters that determine the effective $h_1 h_1 h_2$ interaction. In the conformal regime, $|\sin \alpha|$ is typically tiny, so channels that need sizable h_1 - h_2 mixing or Z - Z' mixing through kinetic mixing are suppressed. Nevertheless, we retain all $2 \rightarrow 2$ contributions in the numerical analysis. To compute the required matrix elements and cross sections, we implement the model in **SARAH** [58] to generate the Feynman rules and export them to **CalcHEP** [59]. Thermal averaging is performed using Eq. (4.9), and the yield in Eq. (4.7) is solved numerically from an initial temperature T_{RH} down to $T \ll M_{N_I}$. We assume T_{RH} is sufficiently high to cover the temperature interval in which production is maximal. If instead T_{RH} is below the relevant mediator thresholds, the resulting abundance is reduced.

A necessary consistency requirement for freeze-in is nonthermalization of the sterile neutrinos with the SM bath. We demand that the N_I production rate $\mathcal{R}(\text{SM SM} \rightarrow N_I N_I)$ be always below the Hubble rate, i.e.,

$$\mathcal{R}(\text{SM SM} \rightarrow N_I N_I) < H(T), \quad (4.12)$$

at all temperatures relevant to DM production. We explicitly verify Eq. (4.12) for all viable scenarios and show $\mathcal{R}(\text{SM SM} \rightarrow N_I N_I)/H$ for two benchmark points with $m_{N_I} = 7 \text{ keV}$ and $m_{N_I} = 100 \text{ keV}$ in Fig. 1. The purple curves represent the contribution from Higgs production, and the orange curve corresponds to production from all SM fermion pairs. In the left panel, the bumps in the production rates originate from the h_1 and h_2 resonances. In the right panel, this feature and production via other SM particles are absent due to the much smaller value of α .

To identify relevant freeze-in DM scenarios consistent with cosmological stability, nonthermalization, and experimental constraints, we perform wide scans over the parameter ranges in Table 2. All parameters are evaluated at the renormalization scale $\mu = 91 \text{ GeV}$. We evolve the renormalization group

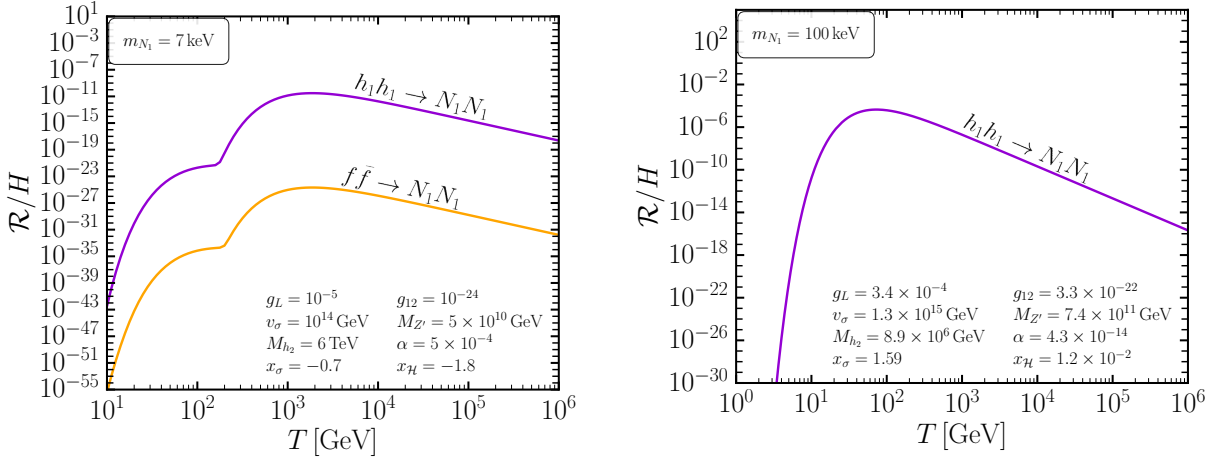


Figure 1: Production rate of N_1 divided by the Hubble expansion rate, $\mathcal{R}(\text{SM SM} \rightarrow N_1 N_1)/H$, as a function of temperature T for two benchmark scenarios. The left panel corresponds to $m_{N_1} = 7 \text{ keV}$, where annihilation into fermionic final states is not very suppressed due to a relatively large value of the scalar mixing parameter α . The right panel corresponds to $m_{N_1} = 100 \text{ keV}$, for which the Higgs channel dominates, and the other production channels are strongly suppressed because α is tiny.

Parameter	Description	Range
M_{h_2}	Heavy scalar mass	$150 \text{ GeV} \lesssim M_{h_2} \lesssim 10^7 \text{ GeV}$
g_L	$U(1)'$ gauge coupling	$10^{-5} \lesssim g_L \lesssim 10^{-3}$
g_{12}	Kinetic mixing coupling	$10^{-25} \lesssim g_{12} \lesssim 10^{-15}$
x_σ	Scalar $U(1)'$ charge	$-5 < x_\sigma < 5$
x_H	Higgs $U(1)'$ charge	$-5 < x_H < 5$
α	Scalar mixing angle	$10^{-23} \lesssim \alpha \lesssim 0.7$
v_σ	Singlet VEV	$5 \times 10^7 \text{ GeV} \lesssim v_\sigma \lesssim 10^{16} \text{ GeV}$
$M_{Z'}$	Dark gauge boson mass	$2 \times 10^5 \text{ GeV} \lesssim M_{Z'} \lesssim 3 \times 10^{13} \text{ GeV}$

Table 2: Input parameter ranges in our numerical scan for models with nonthermal keV neutrino DM produced via freeze-in are shown in the upper part of the table. The output parameters in the bottom three rows are needed for the evaluation of the relic density. All parameters are evaluated at $\mu = 91 \text{ GeV}$.

equations [39] and verify that the model remains perturbative up to the grand unification scale. For each point we (i) impose Eq. (4.12) together with cosmological stability of N_1 , (ii) solve Eq. (4.7) for $Y_{N_1}^\infty$, and (iii) evaluate $\Omega_{N_1} h^2$ via Eq. (4.10). While scenarios beyond the considered parameter ranges may feature nonthermal DM, they are expected to be less relevant phenomenologically. For example, $g_L \lesssim 10^{-5}$ suppresses the interaction strength between N_1 and the SM bath, which in turn reduces the freeze-in efficiency yielding a too small relic density.

By numerically solving Eq. (4.7) for a strong mass hierarchy $M_{N_{2,3}} \gg M_{N_1}$, we obtain the abundance of the lightest sterile neutrino DM N_1 in Fig. 2. All parameter points displayed are consistent with the existing constraints from X-ray observations. The DM relic density, $\Omega_{\text{DM}} h^2 = 0.120 \pm 0.001$, inferred from *Planck* [43], is indicated by the dark grey horizontal line. As mentioned earlier, our model favors small values of the scalar mixing angle $\alpha < 10^{-5}$.

Note that the N_1 production cross sections from SM fermion pairs, provided in Appendix A, are strongly suppressed by the heavy mediator Z' and $g_L \ll 1$. Similarly, the annihilation cross sections to SM vector bosons are suppressed by the mixing angle α . This indicates that the dominant N_1 production channel is via $h_1 h_1 \rightarrow N_1 N_1$, while resonant enhancement occurs when $\sqrt{s} \simeq M_{h_2}$, leading to a localized band of increased yield. In addition, the relevant N_1 couplings entering the production amplitudes are proportional to M_{N_1} in the seesaw/Majoron-like framework, which explains the M_{N_1} -dependence of the

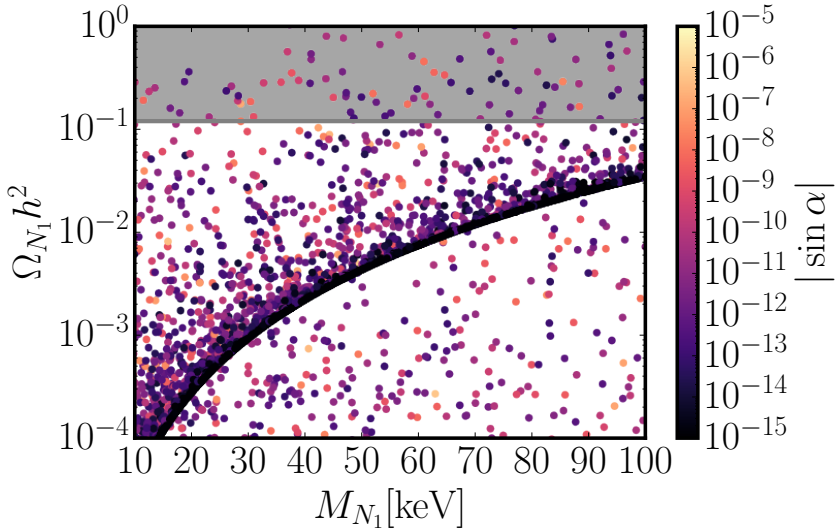


Figure 2: N_1 relic abundance $\Omega_{N_1}h^2$ as a function of the DM mass M_{N_1} for different values of the scalar mixing parameter, $|\sin \alpha|$. All points satisfy the X-ray constraints. The observed relic abundance $\Omega_{N_1}h^2 = 0.12$ is shown as a reference by gray line. Each point corresponds to the numerical solution of the Boltzmann equation (Eq. 4.7) accounting for all relevant dark-to-visible $2 \rightarrow 2$ annihilation channels.

relic abundance. Consequently, for small α , the thermally averaged cross section can be approximated by

$$(n_{h_1}^{\text{eq}})^2 \langle \sigma(h_1 h_1 \rightarrow N_1 N_1) v_r \rangle \simeq \frac{2\pi^2}{(2\pi)^6} \frac{M_{h_1}^4 M_{N_1}^2 T^2}{16\pi v^4} K_1 \left(\frac{M_{h_1}}{T} \right)^2, \quad (4.13)$$

and the resulting freeze-in DM abundance takes the simplified form,

$$\Omega_{N_1} h^2 \simeq 3 \times 10^{-5} \left(\frac{M_{N_1}}{10 \text{ keV}} \right)^3. \quad (4.14)$$

Remarkably, this cubic scaling with M_{N_1} is clearly visible in Fig. 2.

Note that constraints imposed by X-ray searches can be relaxed by allowing for smaller active neutrino masses, which decreases the active-sterile mixing angle and weakens the corresponding bounds. In Fig. 2, the lightest active neutrino takes masses in the range $m_{\nu_1} \in [10^{-12}, 10^{-9}] \text{ eV}$.

5 Lyman- α constraints

The freeze-in production mechanism generates N_1 with a nonthermal momentum distribution. Since primordial velocities suppress clustering below the corresponding freestreaming scale, such scenarios are tightly constrained by the Lyman- α forest, i.e., the absorption pattern in distant quasar spectra produced by neutral hydrogen in the intergalactic medium (IGM). These measurements probe the matter power spectrum down to comoving wavenumbers $k \simeq [0.5-20] h/\text{Mpc}$ and therefore provide some of the most stringent tests of non-cold DM whose primordial velocity distributions suppress structure formation at small scales.

Current Lyman- α analyses are commonly expressed as lower limits on the mass of a *thermal* warm-DM (WDM) relic. These limits depend on the assumed reionization history and on how the thermal evolution of the IGM is modeled. The most stringent limit, obtained from the combined XQ-100 and HIRES/MIKE samples with standard IGM thermal priors [19, 60], requires $m_{\text{WDM}} \gtrsim 5.3 \text{ keV}$ (95% C.L.) if WDM saturates the relic abundance. Allowing for non-monotonic temperature evolution of the IGM relaxes the bound to $m_{\text{WDM}} \gtrsim 3.5 \text{ keV}$ [19], while adopting colder reionization histories that minimize

astrophysical pressure effects weaken it further to $m_{\text{WDM}} \gtrsim 1.9$ keV [60]. We therefore consider two benchmark limits, $m_{\text{WDM}} = 5.3$ keV (stringent) and $m_{\text{WDM}} = 1.9$ keV (conservative), to bracket the associated systematic uncertainties.

To confront our nonthermal N_1 with these limits we compute the linear matter power spectrum $P(k)$ and the corresponding squared transfer function,

$$\mathcal{T}^2(k) \equiv \frac{P(k)}{P_{\Lambda\text{CDM}}(k)}, \quad (5.1)$$

using **CLASS** [61]. ΛCDM is the Λ *cold dark matter* cosmology with Planck's 2018 best-fit parameters [43]. The N_1 momentum distribution resulting from freeze-in is implemented in **CLASS** as a non-cold DM species. For DM produced through $2 \rightarrow 2$ scattering, the phase-space distribution is well approximated by the analytical form [62],

$$f(q) \propto \frac{e^{-q}}{\sqrt{q}}, \quad (5.2)$$

where $q \equiv p/T$. We have explicitly verified by solving the Boltzmann equation that the freeze-in distribution of N_1 follows Eq. (5.2). The overall normalization is fixed for each point in parameter space such that the resulting energy density reproduces the required N_1 abundance.

To quantify the suppression of small-scale power relative to ΛCDM and recast it into thermal-WDM bounds, we adopt the area criterion [62–64], which provides a robust mapping between nonthermal relics and thermal WDM relics constrained by the Lyman- α forest. One first defines the one-dimensional power spectrum,

$$P_{1\text{D}}(k) \approx \frac{1}{2\pi} \int_k^{k_{\text{lim}}} dk' k' P(k'), \quad (5.3)$$

where we take $k_{\text{lim}} = 1.2 \times 10^3 h/\text{Mpc}$ to include the power suppression at the smallest relevant scales, and the corresponding one-dimensional squared transfer function,

$$\mathcal{R}^2(k) = \frac{P_{1\text{D}}(k)}{P_{1\text{D}}^{\Lambda\text{CDM}}(k)}. \quad (5.4)$$

The average loss of small-scale power with respect to ΛCDM is then quantified by

$$\delta A = 1 - \frac{1}{k_{\text{max}} - k_{\text{min}}} \int_{k_{\text{min}}}^{k_{\text{max}}} dk \mathcal{R}^2(k), \quad (5.5)$$

with $k_{\text{min}} = 0.5 h/\text{Mpc}$ and $k_{\text{max}} = 20 h/\text{Mpc}$ corresponding to the MIKE/HIRES + XQ-100 datasets [19]. The quantity δA measures the “missing area” between the ΛCDM and the nonthermal sterile neutrino DM transfer functions on scales probed by the Lyman- α forest. We compare the obtained δA to the reference values δA_{WDM} computed for thermal-WDM relics at the benchmark limits – $m_{\text{WDM}} = 5.3$ keV and $m_{\text{WDM}} = 1.9$ keV – and exclude parameter points for which $\delta A > \delta A_{\text{WDM}}$.

Figure 3 shows $\Omega_{N_1} h^2 / \Omega_{\text{DM}} h^2$ as a function of M_{N_1} . The solid curves correspond to the Lyman- α limits recast from the stringent (red) and conservative (green) thermal WDM limits. The region above each curve is excluded by Lyman- α observations. In the limit that N_1 constitutes all of DM, the stringent bound requires $M_{N_1} \gtrsim 16$ keV, whereas the conservative bound requires $M_{N_1} \gtrsim 3.8$ keV.

6 3.5 keV X-ray line

A particularly intriguing phenomenological target for keV sterile neutrino DM is the weak X-ray feature at $E_\gamma \simeq 3.52 \pm 0.02$ keV in stacked observations of galaxy clusters and individual systems such as the Perseus cluster and M31, with a global significance of about 4.4σ [6, 7].

The line can be interpreted as the monoenergetic photon arising from the two-body radiative transition $N_1 \rightarrow \nu + \gamma$. The dominant contribution to the decay rate is given by Eq. (3.2). The inferred signal region of the parameter space,

$$M_{N_1} \simeq 7 \text{ keV}, \quad \sin^2 2\theta_{\text{eff}} \sim (0.2–2) \times 10^{-10}, \quad (6.1)$$

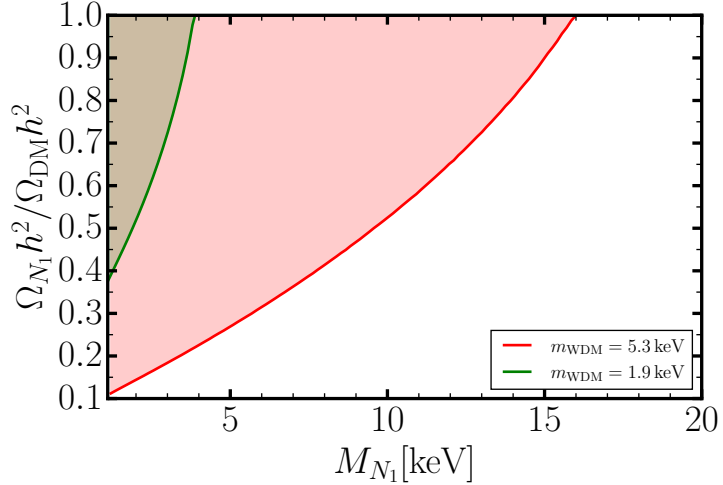


Figure 3: Fraction of the DM abundance contributed by N_1 as a function of M_{N_1} . The curves show the limits derived from Lyman- α forest constraints, using the equivalent thermal WDM masses $m_{\text{WDM}} = 5.3 \text{ keV}$ (red) and $m_{\text{WDM}} = 1.9 \text{ keV}$ (green). The region above each curve is excluded by Lyman- α observations.

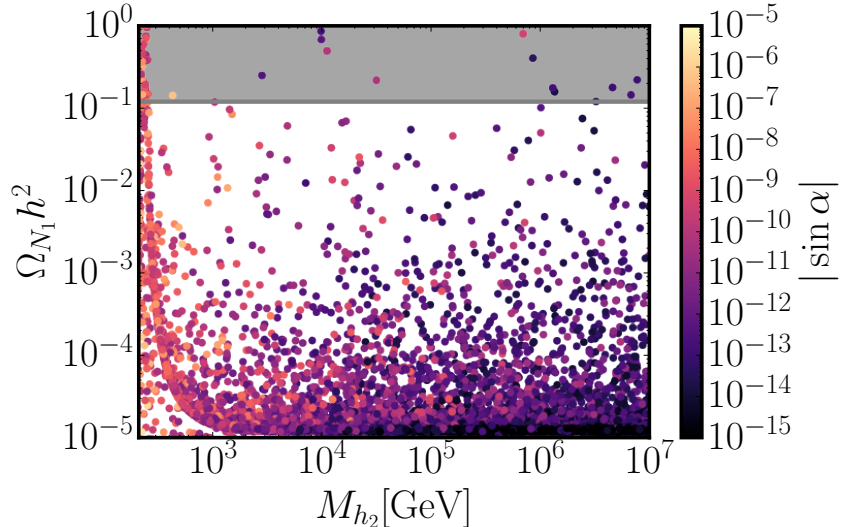


Figure 4: N_1 relic abundance for $M_{N_1} = 7 \text{ keV}$. The color scale shows the corresponding values of the scalar mixing $|\sin \alpha|$. The gray line indicates the inferred DM abundance, $\Omega_{\text{DM}}h^2 \simeq 0.12$. Each point is obtained by solving the Boltzmann equation(Eq. (4.7)) with the thermally averaged annihilation rate including all relevant $2 \rightarrow 2$ production channels.

corresponds to a cosmologically long-lived particle [52]. We treat Eq. (6.1) as a well-motivated benchmark and assess whether our Higgs-dominated freeze-in scenario can simultaneously reproduce the inferred DM relic abundance and the mixing range needed.

The present-day DM abundance for a 7 keV neutrino is shown in Fig. 4 as a function of M_{h_2} , where the color scale indicates the value of $|\sin \alpha|$. Two distinct regimes can be identified.

For $M_{h_2} \lesssim \mathcal{O}(10^3) \text{ GeV}$, relatively larger mixings $|\sin \alpha| \sim \mathcal{O}(10^{-6} - 10^{-5})$ and smaller VEVs $v_\sigma \sim \mathcal{O}(10^{10} - 10^{12}) \text{ GeV}$, are required. This combination does not greatly suppress the interaction between N_1 and the SM bath and therefore enhances the freeze-in production rate. More importantly, for smaller

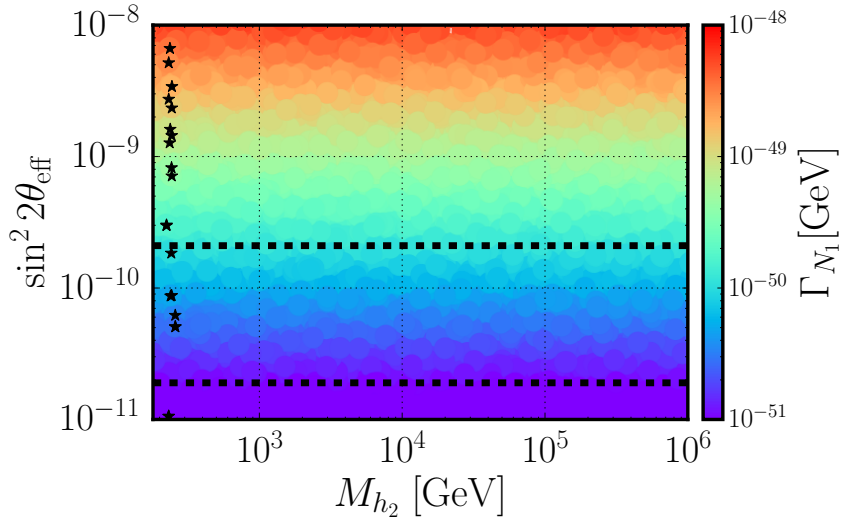


Figure 5: $\sin^2 2\theta_{\text{eff}}$ as a function of M_{h_2} for parameter points satisfying $\Omega_{N_1} h^2 \leq 0.12$. The color scale indicates Γ_{N_1} , and the black stars mark points with $\Omega_{N_1} h^2 = 0.12 \pm 0.001$. The region between dashed lines corresponds to the range $\sin^2 2\theta_{\text{eff}} \simeq (0.2-2) \times 10^{-10}$ needed to produce a 3.5 keV X-ray line via $N_1 \rightarrow \nu\gamma$.

M_{h_2}, N_1 production is resonantly enhanced in the Higgs channel. For the dominant process $h_1 h_1 \rightarrow N_1 N_1$ the threshold $s_{\min} = 4M_{h_1}^2$, and if M_{h_2} is close to the Higgs-pair threshold, $s \simeq M_{h_2}^2 \simeq 4M_{N_1}^2$, yielding a significant enhancement in the thermally averaged cross section and consequently in the freeze-in yield. A small enhancement in production through SM fermions can arise in this region: lowering M_{h_2} correlates with parameter choices that also reduce the effective suppression of the Z' -mediated contribution, thereby increasing the rate for $f\bar{f} \rightarrow N_1 N_1$. However, we find that this contribution remains subdominant with respect to Higgs-initiated production in the parameter space relevant to our 7 keV benchmark, although it contributes to the shape of the region at small values of M_{h_2} .

For $M_{h_2} \gtrsim \mathcal{O}(10^3)$ GeV, v_σ increases and $|\sin \alpha|$ decreases, suppressing the scalar-mediated contribution. Also, the resonance condition $s \simeq M_{h_2}^2$ moves into the large- s tail of the thermal integral, where the Bessel function $K_1(\sqrt{s}/T)$ exponentially suppresses the integrand. As a result, the N_1 abundance rapidly decreases with increasing M_{h_2} and approaches the asymptotic Higgs-dominated regime for large h_2 masses. The viable points then accumulate around $\Omega_{N_1} h^2 \sim 10^{-5}$ for large M_{h_2} , consistent with the scaling in Eq. (4.14).

In Fig. 5 we show $\sin^2 2\theta_{\text{eff}}$ as a function of M_{h_2} for points satisfying $\Omega_{N_1} h^2 \leq 0.12$. The color scale indicates the value of Γ_{N_1} , and the black stars mark the points with $\Omega_{N_1} h^2 = 0.12 \pm 0.001$. The region between the dashed lines corresponds to the mixing angles needed to reproduce the X-ray line at $E_\gamma \simeq 3.5$ keV. The stars accumulate at the Higgs resonance discussed above. Remarkably, some of them fall within the X-ray band. One of these has the following parameters:

$$\begin{aligned} M_{Z'} &= 10^7 \text{ GeV}, & M_{h_2} &= 244 \text{ GeV}, & g_L &= 5.5 \times 10^{-5}, & \alpha &= 9.0 \times 10^{-10}, \\ v_\sigma &= 10^{11} \text{ GeV}, & x_H &= -1.6 \times 10^{-5}, & x_\sigma &= 2, & g_{12} &= 10^{-23}, \end{aligned} \quad (6.2)$$

and provides a natural benchmark for the 7 keV sterile neutrino scenario that simultaneously reproduces the observed relic abundance and the mixing range relevant for the 3.5 keV line.

7 Multi-component decaying dark matter and the S_8 tension

A well-motivated mechanism capable of reducing the predicted clustering amplitude at intermediate scales is *decaying dark matter* (DDM), in which a long-lived parent decays on cosmological time scales

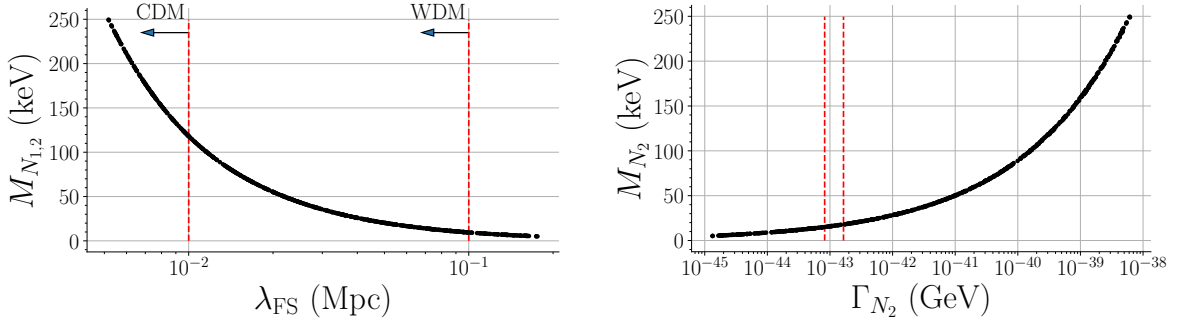


Figure 6: Left: Freestreaming length λ_{FS} of the quasi-degenerate neutrinos N_1 and N_2 . The vertical dashed lines indicate the regions where the sterile neutrinos behave as either cold or warm DM. Right: Mass of the parent sterile neutrino N_2 versus its total decay width Γ_{N_2} ; the vertical dashed lines indicate the decay-width range corresponding to $\tau_{N_2} \sim (4-8) \times 10^{18}$ s.

to a slightly lighter daughter that receives a non-relativistic momentum ‘‘kick’’, thereby suppressing the growth of structure on small scales [65, 66]. Recent DESI-DR1 joint analyses with weak lensing datasets find values of S_8 at the level $S_8 \simeq 0.76-0.79$ (depending on dataset combinations and priors) [30–32], consistent with the range for which DDM-like suppression mechanisms are relevant.

In our framework, this scenario can be realized in a minimal way if at least two keV-scale sterile neutrinos are long-lived. We identify N_2 as the parent state and N_1 as the daughter state. The suppression of the matter power spectrum is controlled primarily by the parent lifetime τ_{N_2} and by the fractional mass splitting, which we parameterize as [65],

$$\epsilon \equiv \frac{1}{2} \left(1 - \frac{M_{N_1}^2}{M_{N_2}^2} \right) \simeq \frac{M_{N_2} - M_{N_1}}{M_{N_2}} \ll 1, \quad M_{N_2} \gtrsim M_{N_1}. \quad (7.1)$$

Physically, ϵ controls the kinetic energy imparted to the daughter and therefore the amount of freestreaming suppression, while τ_{N_2} determines the freestreaming wavenumber.

Following Ref. [65], we identify a representative region that alleviates the S_8 tension characterized by

$$\tau_{N_2} \sim (4-8) \times 10^{18} \text{ s}, \quad \epsilon \sim 0.01-0.1, \quad (7.2)$$

where the precise preferred window depends on the late-time datasets and on the mapping from the power-spectrum suppression to the inferred S_8 . Since the recent results by DESI [30–32] continue to prefer S_8 values in the range for which DDM remains a viable phenomenological option, we adopt Eq. (7.2) as an indicative target region and test whether it can be realized in our model.

Unlike the minimal DDM setups studied in [65, 66], the daughter state N_1 is not stable in our model. Therefore, to determine whether a viable hierarchy of lifetimes can be achieved, we compute all relevant two- and three-body decay channels for both N_2 and N_1 , including $N_I \rightarrow \nu\gamma$, $N_I \rightarrow \nu\bar{\nu}\nu$, and $N_2 \rightarrow N_1\bar{\nu}\nu$. In addition, while the canonical DDM picture assumes a cold parent component, this need not be the case. In the parameter region relevant to Eq. (7.2) both N_1 and N_2 can behave as warm relics. To quantify this, we compute the freestreaming length λ_{FS} following [62] and present the result in Fig. 6 (left). We find that the parent is cold only for $M_{N_2} \gtrsim 120$ keV. Comparing with the decay-width window in Fig. 6 (right), the region compatible with Eq. (7.2) corresponds to a narrow mass interval $M_{N_2} \simeq 15$ keV – 20 keV, which lies in the warm regime.

In this narrow mass range we find that the model can realize a pronounced hierarchy between τ_{N_2} and τ_{N_1} as shown in the left panel of Fig. 7. N_2 decays on cosmological time scales specified by Eq. (7.2), whereas N_1 remains much longer-lived and behaves as a quasi-stable warm particle. In this sense, N_2 plays the role of a decaying warm DM component while N_1 constitutes the effectively stable warm component.¹

¹A study of the impact of this scenario on the matter power spectrum is beyond the scope of this work.

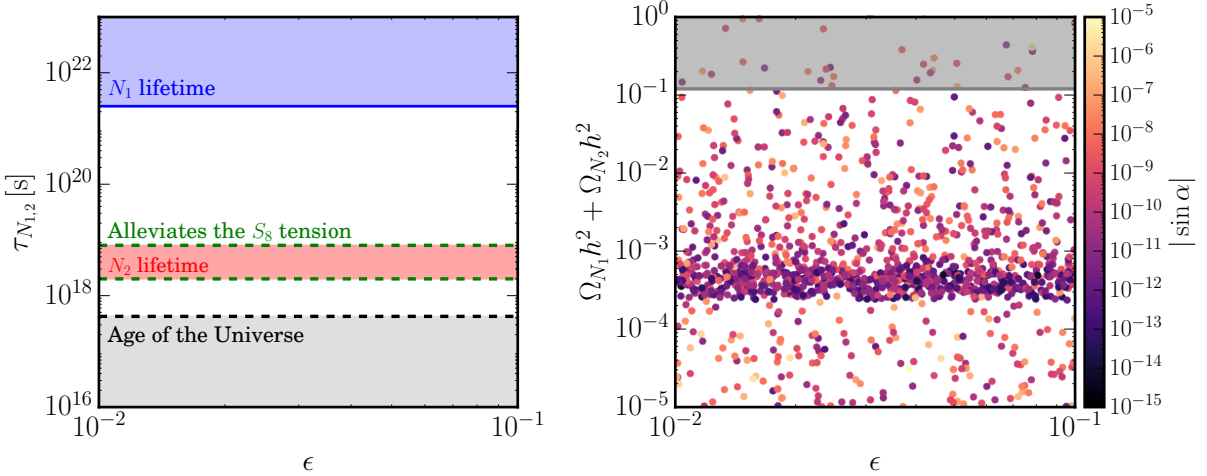


Figure 7: Left: Lifetimes of N_1 and N_2 as functions of the mass-splitting parameter ϵ ; the shaded band highlights the range $\tau_{N_2} \sim (4-8) \times 10^{18}$ s that alleviates the S_8 tension. Right: Relic abundance of the sterile neutrinos for different values of the scalar mixing $|\sin \alpha|$.

Note that the freeze-in picture developed in Section 4 continues to apply. Since N_1 and N_2 are quasi-degenerate and are generated through the same suppressed portals, the freeze-in yields are comparable, and the total sterile neutrino abundance described by Eq. (4.7) can be approximated as $Y \equiv Y_{N_1} + Y_{N_2} \simeq 2Y_{N_2}$, in analogy to the decaying CDM setup of Ref. [65]. Consequently, the total relic density is naturally shared between the two species, with each contributing an $\mathcal{O}(1)$ fraction. Importantly, in the region of parameter space satisfying Eq. (7.2), we find that the correct total relic abundance can be achieved, as illustrated in Fig. 7 (right), while maintaining the required lifetime hierarchy.

8 The KM3NeT event

Before concluding, we briefly note that the conformal $U(1)'$ framework can also accommodate much heavier sterile neutrino DM candidates, in a different corner of parameter space. This possibility has attracted attention following the KM3NeT event, KM3-230213A, a track-like signature compatible with an ultra-high-energy muon of reconstructed energy $E_\mu = 120^{+110}_{-60}$ PeV [34]. The parent neutrino energy is inferred to be in the broad range $E_\nu \sim 110$ PeV – 790 PeV (at 1σ), with a median of 220 PeV [34]. If the event is interpreted as originating from the two-body decay of a superheavy DM particle into light neutrinos, the characteristic mass scale is set by $M_{\text{DM}} \sim 2E_\nu$, pointing to $M_{\text{DM}} \sim 440$ PeV.

We find that our model can reproduce such a heavy sterile neutrino. However, this solution requires an extreme amount of fine-tuning because the DM needs to be exceptionally long-lived, which in a minimal type-I seesaw realization corresponds to ultra-suppressed active-sterile Yukawa couplings. Using $y_\nu \sim \mathcal{O}(10^{-31})$ for $M_{N_1} \simeq 440$ PeV, we find (in the absence of flavor cancellations) the scale of the lightest neutrino mass to be

$$m_\nu \sim \frac{y_\nu^2 v^2}{2M_{N_1}} \sim 10^{-56} \text{ eV}, \quad (8.1)$$

which illustrates the degree of tuning required.

In addition, unlike the freeze-in production mechanism discussed in Section 4 for keV DM, the relic density for $M_{N_1} \simeq 440$ PeV cannot be efficiently generated through the same $2 \rightarrow 2$ bath processes. In our model, $M_{Z'} > M_{h_2}$, so that $h_2 \rightarrow N_1 \bar{N}_1$ is the only efficient production mode with h_2 effectively acting as the reheating/inflaton field. Obtaining the correct relic abundance then requires the decay to occur extremely close to threshold, with a relative mass splitting,

$$\frac{M_{h_2} - 2M_{N_1}}{M_{h_2}} \sim 10^{-12}, \quad (8.2)$$

so that phase-space suppression compensates the otherwise excessive population of N_1 from h_2 decays.

9 Summary

We studied a classically conformal $U(1)'$ extension of the SM in which the lightest sterile neutrino, N_1 , is a feebly interacting dark-matter (DM) candidate produced via freeze-in. The conformal symmetry forbids explicit mass scales in the tree-level Lagrangian, and the full spectrum, including the $U(1)'$ gauge boson Z' and the singlet-like scalar h_2 , is generated dynamically via radiative corrections. In the minimal keV-DM setup, N_1 is the only long-lived sterile state. If the next-to-lightest sterile neutrino N_2 is also long-lived, the model naturally realizes multi-component DM produced via freeze-in with late-time decays.

We performed a numerical calculation of the sterile neutrino abundance by solving the Boltzmann equation for freeze-in production, scanning the parameter space and identifying regions consistent with the observed relic density, $\Omega_{\text{DM}} h^2 \simeq 0.12$. We implemented the corresponding nonthermal phase-space distribution in the Boltzmann solver `CLASS` and computed the linear matter power spectrum. We interpreted Lyman- α forest constraints through the thermal-equivalent WDM benchmarks, and found that the predicted suppression of small-scale power is compatible with both stringent and conservative limits, $m_{\text{WDM}}^{\text{th}} = 5.3$ keV and 1.9 keV, respectively, within the viable freeze-in parameter space.

In the keV mass range, the radiative decay $N_1 \rightarrow \nu\gamma$ provides a clear X-ray line signal. In particular, for $M_{N_1} = 7$ keV we identified a viable parameter region that simultaneously reproduces the inferred DM abundance and the effective mixing angle relevant for interpreting the unidentified line at $E_\gamma \simeq 3.5$ keV observed in galaxy clusters as due to $N_1 \rightarrow \nu\gamma$ decays.

If both N_1 and N_2 are long-lived, the model realizes a decaying (multi-component) DM setup in which the late decay $N_2 \rightarrow N_1 + (\text{light states})$ injects a small velocity dispersion for the daughter particle and can suppress the growth of structure on small scales. We demonstrated that the parameter space can accommodate the indicated lifetime and mass-splitting window relevant for alleviating the S_8 tension, while reproducing the correct relic abundance.

Finally, we commented on a corner of parameter space in which the decay of a 440 PeV sterile neutrino N_1 , being the lightest in the Majorana neutrino spectrum, can play the role of DM and explain the KM3NeT event, KM3-230213A. However, an exceptional degree of fine-tuning in the neutrino-sector parameters and in the nonthermal cosmological history (notably, near-threshold production from h_2 decays) is required. We, therefore, regard the keV-scale freeze-in scenario as the most robust and predictive regime of the model.

Acknowledgments

D.M. is supported in part by the U.S. Department of Energy under Grant No. DE-SC0010504. A.P.M. is supported by FCT through the project with reference 2024.05617.CERN (<https://doi.org/10.54499/2024.05617.CERN>). J.G. and A.P.M. are also supported by LIP and FCT, reference LA/P/0016/2020 (<https://doi.org/10.54499/LA/P/0016/2020>) and by the ERC-PT A-Projects 'Unveiling', financed by PRR, NextGenerationEU. V.O. is directly funded by FCT through the doctoral program grant with the reference PRT/BD/154629/2022 (<https://doi.org/10.54499/PRT/BD/154629/2022>). V.O. also acknowledges support by the COST Action CA21106 (Cosmic WISPerS).

A Production cross sections for light dark matter

In the freeze-in regime, the sterile neutrino relic abundance is sourced by feeble $2 \rightarrow 2$ processes involving SM particles in the thermal bath. For analytic insight, we consider the parametric limit

$$M_{N_1} \ll M_{\text{SM}}, \quad |\alpha| \ll 1, \quad (\text{A.1})$$

and retain only the leading contributions from s -channel exchange. The expressions below are order-of-magnitude approximations that reproduce the qualitative behavior and the numerical trends of the full computation in the relevant parameter space. Here, s denotes the usual Mandelstam variable, and mediator widths in the propagators can be reinstated by the substitution, $M^2 \rightarrow M^2 - iM\Gamma$.

We list production cross sections in the limit $M_{N_1} \rightarrow 0$. Then, the dependence on M_{N_1} in the kinematics is negligible, while the overall coupling strength remains controlled by the feeble portals.

$$\sigma_{\ell^+ \ell^- \rightarrow N_1 N_1} \simeq \frac{g_L^4 x_\sigma^2}{384\pi} \frac{s(10x_h^2 + 6x_h x_\sigma + x_\sigma^2)}{(s - M_{Z'}^2)^2}, \quad (\text{A.2})$$

$$\sigma_{\nu_\ell \bar{\nu}_\ell \rightarrow N_1 N_1} \simeq \frac{g_L^4 x_\sigma^2}{384\pi} \frac{s(2x_h + x_\sigma)^2}{(s - M_{Z'}^2)^2}, \quad (\text{A.3})$$

$$\sigma_{h_1 h_1 \rightarrow N_1 N_1} \simeq \frac{M_{h_2}^4 M_{N_1}^2}{4\pi v^4} \frac{s(s - M_{h_1}^2)}{(M_{h_2}^2 - s)^2 (M_{h_1}^2 - s)^2} \sqrt{1 - \frac{4M_{h_1}^2}{s}}, \quad (\text{A.4})$$

$$\sigma_{q_u \bar{q}_u \rightarrow N_1 N_1} \simeq \frac{g_L^4 x_\sigma^2}{10368\pi} \frac{s(34x_h^2 + 19x_h x_\sigma + x_\sigma^2)}{(M_{Z'}^2 - s)^2}, \quad (\text{A.5})$$

$$\sigma_{q_d \bar{q}_d \rightarrow N_1 N_1} \simeq \frac{g_L^4 x_\sigma^2}{10368\pi} \frac{s(10x_h^2 - 2x_h x_\sigma + x_\sigma^2)}{(M_{Z'}^2 - s)^2}. \quad (\text{A.6})$$

Here, ℓ denotes a charged lepton, ν_ℓ the corresponding active neutrino flavor, and $q_{u,d}$ up- and down-type quarks with masses $m_{q_{u,d}}$. The phase-space factors in final states with massive particles are adequate approximations. Additional velocity-suppressed terms are negligible in the limit considered.

Note that production initiated by SM gauge bosons (ZZ , W^+W^-) is strongly suppressed in the freeze-in regime because the relevant amplitudes are proportional to the scalar mixing angle. In particular, for h_2 -mediated production the coupling to SM gauge bosons inherits a mixing suppression $\propto \sin \alpha$, implying the cross sections scaling as $\propto \sin^2 \alpha$ (and in several channels as $\propto \sin^2 2\alpha$ depending on the interference structure). Since the phenomenologically viable region for freeze-in satisfies $|\alpha| \ll 1$, these gauge boson contributions are several orders of magnitude smaller than the dominant channels listed and can be neglected.

References

- [1] A. Boyarsky, M. Drewes, T. Lasserre, S. Mertens, and O. Ruchayskiy, *Sterile neutrino Dark Matter*, *Prog. Part. Nucl. Phys.* **104** (2019) 1–45.
- [2] P. B. Pal and L. Wolfenstein, *Radiative Decays of Massive Neutrinos*, *Phys. Rev. D* **25** (1982) 766.
- [3] D. Barret *et al.*, *The Athena X-ray Integral Field Unit*, *Proc. SPIE Int. Soc. Opt. Eng.* **10699** (2018) 106991G, [[1807.06092](#)].
- [4] **eROSITA** Collaboration, A. Merloni *et al.*, *eROSITA Science Book: Mapping the Structure of the Energetic Universe*, [1209.3114](#).
- [5] **XRISM Science Team** Collaboration, *Science with the X-ray Imaging and Spectroscopy Mission (XRISM)*, [2003.04962](#).
- [6] E. Bulbul, M. Markevitch, A. Foster, R. K. Smith, M. Loewenstein, and S. W. Randall, *Detection of An Unidentified Emission Line in the Stacked X-ray spectrum of Galaxy Clusters*, *Astrophys. J.* **789** (2014) 13, [[1402.2301](#)].
- [7] A. Boyarsky, O. Ruchayskiy, D. Iakubovskyi, and J. Franse, *Unidentified Line in X-Ray Spectra of the Andromeda Galaxy and Perseus Galaxy Cluster*, *Phys. Rev. Lett.* **113** (2014) 251301, [[1402.4119](#)].
- [8] H. Stiele, W. Pietsch, F. Haberl, D. Hatzidimitriou, R. Barnard, B. F. Williams, A. K. H. Kong, and U. Kolb, *The deepxmm-newtonsurvey of m31*, *Astronomy & Astrophysics* **534** (Oct., 2011) A55.
- [9] S. Dodelson and L. M. Widrow, *Sterile-neutrinos as dark matter*, *Phys. Rev. Lett.* **72** (1994) 17–20, [[hep-ph/9303287](#)].
- [10] A. D. Dolgov and S. H. Hansen, *Massive sterile neutrinos as warm dark matter*, *Astropart. Phys.* **16** (2002) 339–344, [[hep-ph/0009083](#)].
- [11] A. Boyarsky, A. Neronov, O. Ruchayskiy, and M. Shaposhnikov, *Constraints on sterile neutrino as a dark matter candidate from the diffuse x-ray background*, *Mon. Not. Roy. Astron. Soc.* **370** (2006) 213–218, [[astro-ph/0512509](#)].
- [12] C. R. Watson, J. F. Beacom, H. Yuksel, and T. P. Walker, *Direct X-ray Constraints on Sterile Neutrino Warm Dark Matter*, *Phys. Rev. D* **74** (2006) 033009, [[astro-ph/0605424](#)].
- [13] M. Loewenstein and A. Kusenko, *Dark Matter Search Using Chandra Observations of Willman 1, and a Spectral Feature Consistent with a Decay Line of a 5 keV Sterile Neutrino*, *Astrophys. J.* **714** (2010) 652–662, [[0912.0552](#)].
- [14] O. Urban, N. Werner, S. W. Allen, A. Simionescu, J. S. Kaastra, and L. E. Strigari, *A Suzaku Search for Dark Matter Emission Lines in the X-ray Brightest Galaxy Clusters*, *Mon. Not. Roy. Astron. Soc.* **451** (2015), no. 3 2447–2461, [[1411.0050](#)].
- [15] H. Yuksel, J. F. Beacom, and C. R. Watson, *Strong Upper Limits on Sterile Neutrino Warm Dark Matter*, *Phys. Rev. Lett.* **101** (2008) 121301, [[0706.4084](#)].
- [16] A. Boyarsky, D. Malyshev, A. Neronov, and O. Ruchayskiy, *Constraining DM properties with SPI*, *Mon. Not. Roy. Astron. Soc.* **387** (2008) 1345, [[0710.4922](#)].
- [17] A. Neronov, D. Malyshev, and D. Eckert, *Decaying dark matter search with NuSTAR deep sky observations*, *Phys. Rev. D* **94** (2016), no. 12 123504, [[1607.07328](#)].
- [18] K. Perez, K. C. Y. Ng, J. F. Beacom, C. Hersh, S. Horiuchi, and R. Krivonos, *Almost closing the ν MSM sterile neutrino dark matter window with NuSTAR*, *Phys. Rev. D* **95** (2017), no. 12 123002, [[1609.00667](#)].
- [19] V. Iršič *et al.*, *New Constraints on the free-streaming of warm dark matter from intermediate and small scale Lyman- α forest data*, *Phys. Rev. D* **96** (2017), no. 2 023522, [[1702.01764](#)].
- [20] K. N. Abazajian, *Sterile neutrinos in cosmology*, *Phys. Rept.* **711-712** (2017) 1–28, [[1705.01837](#)].
- [21] J. Baur, N. Palanque-Delabrouille, C. Y. Ng, J. F. Beacom, C. Hersh, S. Horiuchi, and R. Krivonos, *Almost closing the ν MSM sterile neutrino dark matter window with NuSTAR*, *Phys. Rev. D* **95** (2017), no. 12 123002, [[1609.00667](#)].
- [22] A. Boyarsky, O. Ruchayskiy, and D. Iakubovskyi, *A Lower bound on the mass of Dark Matter particles*, *JCAP* **03** (2009) 005, [[0808.3902](#)].

[23] A. Boyarsky, J. Lesgourgues, O. Ruchayskiy, and M. Viel, *Lyman-alpha constraints on warm and on warm-plus-cold dark matter models*, *JCAP* **05** (2009) 012, [[0812.0010](#)].

[24] O. Ruchayskiy, A. Boyarsky, D. Iakubovskyi, E. Bulbul, D. Eckert, J. Franse, D. Malyshev, M. Markevitch, and A. Neronov, *Searching for decaying dark matter in deep XMM-Newton observation of the Draco dwarf spheroidal*, *Mon. Not. Roy. Astron. Soc.* **460** (2016), no. 2 1390–1398, [[1512.07217](#)].

[25] J. Franse *et al.*, *Radial Profile of the 3.55 keV line out to R_{200} in the Perseus Cluster*, *Astrophys. J.* **829** (2016), no. 2 124, [[1604.01759](#)].

[26] N. Cappelluti, E. Bulbul, A. Foster, P. Natarajan, M. C. Urry, M. W. Bautz, F. Civano, E. Miller, and R. K. Smith, *Searching for the 3.5 keV Line in the Deep Fields with Chandra: the 10 Ms observations*, *Astrophys. J.* **854** (2018), no. 2 179, [[1701.07932](#)].

[27] **XRISM** Collaboration, M. Audard *et al.*, *XRISM Constraints on Unidentified X-Ray Emission Lines, Including the 3.5 keV Line, in the Stacked Spectrum of 10 Galaxy Clusters*, *Astrophys. J. Lett.* **994** (2025), no. 1 L28, [[2510.24560](#)].

[28] C. Dessert, J. W. Foster, Y. Park, and B. R. Safdi, *Was There a 3.5 keV Line?*, *Astrophys. J.* **964** (2024), no. 2 185, [[2309.03254](#)].

[29] S. Oda, N. Okada, and D.-s. Takahashi, *Classically conformal $U(1)'$ extended standard model and Higgs vacuum stability*, *Phys. Rev. D* **92** (2015), no. 1 015026, [[1504.06291](#)].

[30] A. Porredon *et al.*, *DESI-DR1 3 \times 2-pt analysis: consistent cosmology across weak lensing surveys*, [2512.15960](#).

[31] A. Semenaite *et al.*, *Joint cosmological fits to DESI-DR1 full-shape clustering and weak gravitational lensing in configuration space*, [2512.15961](#).

[32] J. U. Lange *et al.*, *Cosmological Constraints from Full-Scale Clustering and Galaxy-Galaxy Lensing with DESI DR1*, [2512.15962](#).

[33] E. Abdalla *et al.*, *Cosmology intertwined: A review of the particle physics, astrophysics, and cosmology associated with the cosmological tensions and anomalies*, *JHEAp* **34** (2022) 49–211, [[2203.06142](#)].

[34] **KM3NeT** Collaboration, S. Aiello *et al.*, *Observation of an ultra-high-energy cosmic neutrino with KM3NeT*, *Nature* **638** (2025), no. 8050 376–382. [Erratum: *Nature* 640, E3 (2025)].

[35] K. Kohri, P. K. Paul, and N. Sahu, *Super heavy dark matter origin of the PeV neutrino event: KM3-230213A*, [2503.04464](#).

[36] Y. Chikashige, R. N. Mohapatra, and R. D. Peccei, *Spontaneously Broken Lepton Number and Cosmological Constraints on the Neutrino Mass Spectrum*, *Phys. Rev. Lett.* **45** (1980) 1926.

[37] Y. Chikashige, R. N. Mohapatra, and R. D. Peccei, *Are There Real Goldstone Bosons Associated with Broken Lepton Number?*, *Phys. Lett. B* **98** (1981) 265–268.

[38] G. B. Gelmini and M. Roncadelli, *Left-Handed Neutrino Mass Scale and Spontaneously Broken Lepton Number*, *Phys. Lett. B* **99** (1981) 411–415.

[39] J. Gonçalves, D. Marfatia, A. P. Morais, and R. Pasechnik, *Gravitational waves from supercooled phase transitions in conformal Majoron models of neutrino mass*, *JHEP* **02** (2025) 110, [[2412.02645](#)].

[40] J. A. Casas and A. Ibarra, *Oscillating neutrinos and $\mu \rightarrow e, \gamma$* , *Nucl. Phys. B* **618** (2001) 171–204.

[41] I. Cordero-Carrión, M. Hirsch, and A. Vicente, *General parametrization of Majorana neutrino mass models*, *Phys. Rev. D* **101** (2020), no. 7 075032.

[42] I. Esteban, M. C. Gonzalez-Garcia, M. Maltoni, I. Martinez-Soler, J. P. Pinheiro, and T. Schwetz, *NuFit-6.0: updated global analysis of three-flavor neutrino oscillations*, *JHEP* **12** (2024) 216, [[2410.05380](#)].

[43] **Planck** Collaboration, N. Aghanim *et al.*, *Planck 2018 results. VI. Cosmological parameters*, *Astron. Astrophys.* **641** (2020) A6, [[1807.06209](#)]. [Erratum: *Astron. Astrophys.* 652, C4 (2021)].

[44] **ATLAS** Collaboration, G. Aad *et al.*, *Combined Measurement of the Higgs Boson Mass from the $H \rightarrow \gamma\gamma$ and $H \rightarrow ZZ^* \rightarrow 4l$ Decay Channels with the ATLAS Detector Using $s=7, 8,$ and 13 TeV pp Collision Data*, *Phys. Rev. Lett.* **131** (2023), no. 25 251802, [[2308.04775](#)].

[45] **ATLAS** Collaboration, G. Aad *et al.*, *A detailed map of Higgs boson interactions by the ATLAS experiment ten years after the discovery*, *Nature* **607** (2022), no. 7917 52–59, [[2207.00092](#)]. [Erratum: *Nature* 612, E24 (2022)].

[46] **ATLAS** Collaboration, G. Aad *et al.*, *Search for $t\bar{t}$ resonances in fully hadronic final states in pp collisions at $\sqrt{s} = 13$ TeV with the ATLAS detector*, *JHEP* **10** (2020) 061, [[2005.05138](#)].

[47] **ATLAS** Collaboration, G. Aad *et al.*, *Search for lepton-flavour violation in high-mass dilepton final states using 139 fb^{-1} of pp collisions at $\sqrt{s} = 13$ TeV with the ATLAS detector*, *JHEP* **23** (2020) 082, [[2307.08567](#)].

[48] **CMS** Collaboration, A. Hayrapetyan *et al.*, *Search for a Neutral Gauge Boson with Nonuniversal Fermion Couplings in Vector Boson Fusion Processes in Proton-Proton Collisions at $s=13$ TeV*, *Phys. Rev. Lett.* **135** (2025), no. 6 061803, [[2412.19261](#)].

[49] V. V. Khoze, C. McCabe, and G. Ro, *Higgs vacuum stability from the dark matter portal*, *JHEP* **08** (2014) 026, [[1403.4953](#)].

[50] J. C. Helo, S. Kovalenko, and I. Schmidt, *Sterile neutrinos in lepton number and lepton flavor violating decays*, *Nucl. Phys. B* **853** (2011) 80–104, [[1005.1607](#)].

[51] V. D. Barger, R. J. N. Phillips, and S. Sarkar, *Remarks on the KARMEN anomaly*, *Phys. Lett. B* **352** (1995) 365–371, [[hep-ph/9503295](#)]. [Erratum: *Phys.Lett.B* 356, 617–617 (1995)].

[52] M. Drewes *et al.*, *A White Paper on keV Sterile Neutrino Dark Matter*, *JCAP* **01** (2017) 025, [[1602.04816](#)].

[53] J. Alwall, R. Frederix, S. Frixione, V. Hirschi, F. Maltoni, O. Mattelaer, H. S. Shao, T. Stelzer, P. Torrielli, and M. Zaro, *The automated computation of tree-level and next-to-leading order differential cross sections, and their matching to parton shower simulations*, *JHEP* **07** (2014) 079, [[1405.0301](#)].

[54] H. Yüksel, J. F. Beacom, and C. R. Watson, *Strong upper limits on sterile neutrino warm dark matter*, *Phys. Rev. Lett.* **101** (Sep, 2008) 121301.

[55] L. J. Hall, K. Jedamzik, J. March-Russell, and S. M. West, *Freeze-In Production of FIMP Dark Matter*, *JHEP* **03** (2010) 080, [[0911.1120](#)].

[56] P. Gondolo and G. Gelmini, *Cosmic abundances of stable particles: Improved analysis*, *Nucl. Phys. B* **360** (1991) 145–179.

[57] **Particle Data Group** Collaboration, S. Navas *et al.*, *Review of particle physics*, *Phys. Rev. D* **110** (2024), no. 3 030001.

[58] F. Staub, *SARAH 4 : A tool for (not only SUSY) model builders*, *Comput. Phys. Commun.* **185** (2014) 1773–1790, [[1309.7223](#)].

[59] A. Belyaev, N. D. Christensen, and A. Pukhov, *CalcHEP 3.4 for collider physics within and beyond the Standard Model*, *Comput. Phys. Commun.* **184** (2013) 1729–1769, [[1207.6082](#)].

[60] A. Garzilli, A. Magalich, O. Ruchayskiy, and A. Boyarsky, *How to constrain warm dark matter with the Lyman- α forest*, *Mon. Not. Roy. Astron. Soc.* **502** (2021), no. 2 2356–2363, [[1912.09397](#)].

[61] D. Blas, J. Lesgourgues, and T. Tram, *The cosmic linear anisotropy solving system (class). part ii: Approximation schemes*, *Journal of Cosmology and Astroparticle Physics* **2011** (2011), no. 07 034.

[62] F. D'Eramo and A. Lenoci, *Lower mass bounds on FIMP dark matter produced via freeze-in*, *JCAP* **10** (2021) 045, [[2012.01446](#)].

[63] A. Schneider, *Astrophysical constraints on resonantly produced sterile neutrino dark matter*, *JCAP* **04** (2016) 059, [[1601.07553](#)].

[64] R. Murgia, A. Merle, M. Viel, M. Totzauer, and A. Schneider, *”Non-cold” dark matter at small scales: a general approach*, *JCAP* **11** (2017) 046, [[1704.07838](#)].

[65] L. Fuß, M. Garny, and A. Ibarra, *Minimal decaying dark matter: from cosmological tensions to neutrino signatures*, *JCAP* **01** (2025) 055, [[2403.15543](#)].

[66] M. D. Astros, L. Gráf, and S. Vogl, *Less structure on 8 Mpc scales from decaying sterile neutrino dark matter*, [2511.22638](#).